CHAPTER

4
Degradation by metal–doped g–C_3N_4

1. Introduction

In recent years, there has been a notable increase in the use of dyes, resulting in a significant discharge of dye-based waste into water bodies. This discharge has adversely affected water quality, soil health, and the overall well–being of both plant and animal life, thereby impacting human populations (Priyadarshan et. al., 2023). Among the various types of dyes produced, azo dyes are particularly noteworthy due to their extensive use, stability, and heightened levels of toxicity (Maurya el al., 2021).

Titanium dioxide (TiO_2) has emerged as a widely used photocatalyst for various applications, including dye degradation (Khajavian et. al., 20017), pharmaceutical waste removal (Hernandez- Uresti et. al., 2016), and energy generation (Y. Wang et. al., 2017) when exposed to UV light. However, it is important to recognize that harnessing the potential of TiO_2 can be expensive, primarily because a considerable portion of solar radiation received at the Earth's surface comprises visible light (43%) and infrared light (52%) (Z. Song et. al.,2016). This economic challenge may hinder the widespread utilization of TiO_2 for these purposes.

Also highlighted in Sustainable Development Goal (SDG) 6 by the UN, the provision of clean water and adequate sanitation is imperative. The utilization of g–C_3N_4, which exhibits photocatalytic activity under sunlight, addresses this goal. Being a metal–free organic semiconductor (Yadav and Yadav, 2024), g–C_3N_4 is active under both UV and visible light (Dhar et. al., 2023), garnering increasing global attention as a photocatalyst (Y. Gong et. al., 2015). Over the past few decades, research on g–C_3N_4 has surged, indicating its growing significance (F. Chang et. al., 2013). Despite requiring complex and costly fabrication steps for modification, these processes are unsuitable for large–scale industrial applications. Hence, there is a pressing need to develop new photocatalysts that are easy to manufacture and offer improved applicability. In more specific terms, g–C_3N_4 is a semiconductor with a narrow band gap (2.7 eV), enabling it to absorb blue light up to 450 nm (J. Li et. al., 2012). This favorable band gap, coupled with its thermal and chemical stability, makes it particularly well–suited for applications in photochemistry and photocatalysis (K. Cao et. al., 2015). However, most of the electrons getting generated is recombined with holes. To abate this recombination process, doing is applied. Here we have taken few metals. Doping in photocatalysts is done to enhance their performance by modifying their electronic structure. Transition metals are used as dopants in photocatalysts to enhance their efficiency by improving light absorption, charge carrier separation, and redox reactions. Metals like Fe, Co, Cu etc, introduce mid-gap states, extend absorption into the visible range, and reduce recombination, thereby boosting photocatalytic performance in energy and environmental applications.

2. Experimental

All the materials and chemicals used during the experiment were melamine for the synthesis of g–C_3N_4; $FeSO_4$, $CoSO_4$ and $NiSO_4(H_2O)_6$ for fabrication of corresponding metal doped g–C_3N_4 were purchased from SDFCL, Mumbai, India and Congo red (CR) ($C_{32}H_{22}N_6O_6S_2Na$) was supplied from SRL, Taloja, India. All the precursors were of laboratory grade and used without further purification. Distilled water was used in each step.

Synthesis of all photocatalysts was by thermal condensation method with melamine of fixed quantity as a precursor at 600^0C for 6h (A. Pilai et. al.,2022). Figure. 4.1 showing the formation and changes due to doping of metal. The resulting yellow powder was washed with Et(OH) and then water to ensure the removal of any impurity or any reaction intermediate present (Y. Wang et. al., 2012). The same process was repeated with the addition of a metal compound (5% wt. of melamine) with melamine. To ensure proper mixing, 10 ml water was added to form a slurry (Selvam et. al., 2018). The photocatalytic activity of g–C_3N_4 was monitored using photoreactor equipped with visible light by choosing a common hazardous pollutant, solution of congo red (CR) dye. Before the start of the photocatalytic reaction, a photocatalyst is added to the solution to meet the adsorption–desorption equilibrium (Sobhani-Nasab et. al., 2019). After completion of the reaction, the solution is centrifuged at a constant speed for 5 minutes to separate the particles of the photocatalyst (X. Song et al, 2014). The concentration of CR was metered by UV–Vis spectrophotometer at 497nm (Mohini and Lakshminarasimhan, 2016).

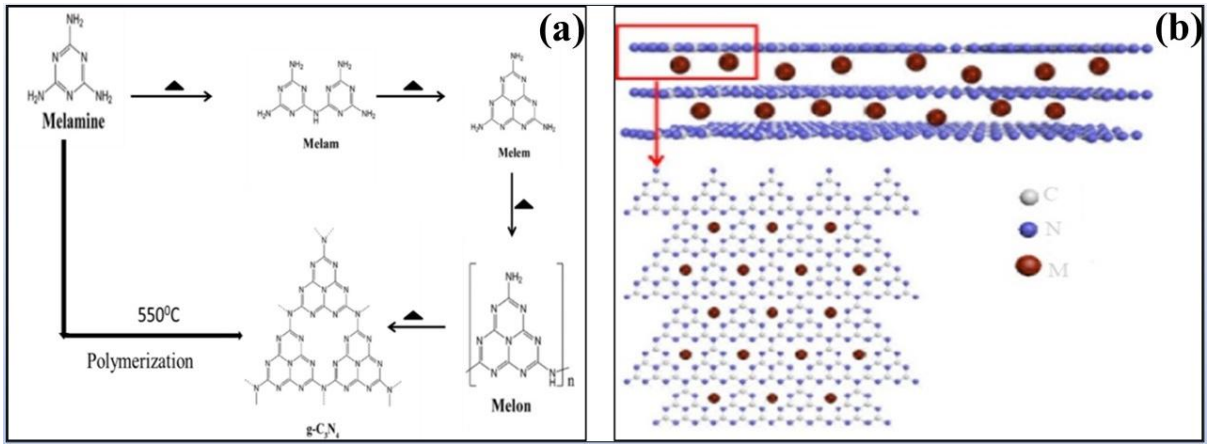

Figure 4.1 Formation of (a) pure g–C_3N_4 and (b) Change in structure after metal introduction

3. Characterization

For X–ray diffraction (XRD) spectra Rigaku, Lead equipment was used to examine the structure of the catalyst. SEM images were captured with JCM–6000 Plus Bench Top Sem Neoscope by JEOL Asia PTE Ltd. FTIR spectra were plotted with Nicolet iS5 by THERMO Electron Scientific Instruments LLC model no. BELLSORP MAX II & BELCAT–II by MicrotracBEL Corp instrument was used to obtain the adsorption–desorption isotherms data and EDX testing is performed to find the presence of metal–doped in the catalyst. EDX was done with Quanta 450, EDAX. DRS was done to find and determine the band gap with help of a Tauc plot with the help of absorbance with changing wavelength in a UV–Visible Spectrophotometer.

3.1 XRD

XRD pattern shows the presence of the hexagonal ring at 13.4° corresponding to millers indices (100) and the sharp peak obtained was due to carbon at 27.4° (200) in figure (a) with the presence of metals in their oxides form corresponding to the metal line and compared with pure g–C_3N_4. Peaks at (002) and (100) are present in doped powders also

but small peaks eg. at 22° in g–C_3N_4/Fe and g–C_3N_4/Co catalyst and 43° in g–C_3N_4/Ni are corresponding to metal sulfates. Peak at 13.2° gets intensified in case of doped, this ensures the better formation of g–C_3N_4 which is responsible for photocatalysis and formation of different metal oxides are responsible for abatement of recombination.

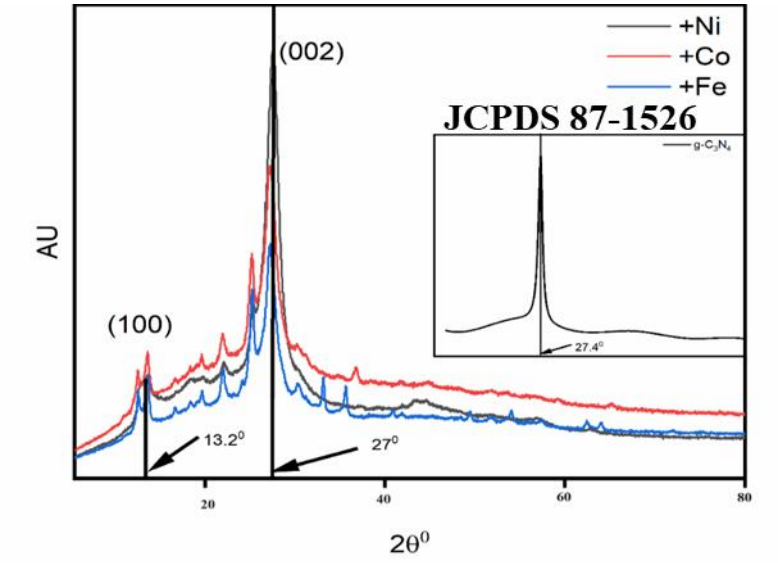

Figure 4.2 XRD pattern of g–C_3N_4 doped with metal and (inset) g–C_3N_4

3.2 FTIR analysis

Figure 25 illustrates the FTIR spectra of the nanocomposites g–C_3N_4/Fe, g–C_3N_4/Co, and g–C_3N_4/Ni, verifying their presence in powdered form, primarily as oxides. The spectra unveil distinctive characteristics, including a significant broad band within the range of 3100–3400 cm^{-1}, attributable to the presence of moisture (Dharela et. al., 2022). This can be ascribed to the stretching vibrations of primary (*–NH_2*) and secondary (*–NH–)* amines, originating from residual amino groups situated at the peripheries of the heterocyclic CN structure.

Furthermore, a peak observed at 1250 cm^{-1} indicates the presence of *–CN–* in amide within g–C_3N_4, which diminishes following a specific treatment, likely attributable to the substitution of a nitrogen atom with a metal atom. Notably, various absorption

peaks within the range of 1200–1640 cm^{-1} can be linked to the stretching vibrations of *C–N* bonds and the *C–N* bonds within the *CN* aromatic repeating unit. Additionally, distinct out–of–plane vibrations associated with the triazine/s–triazine aromatic repeating units are affirmed by absorption peaks at wavenumbers of 885 cm^{-1} and 800 cm^{-1} (Bledowski et. al., 2011).

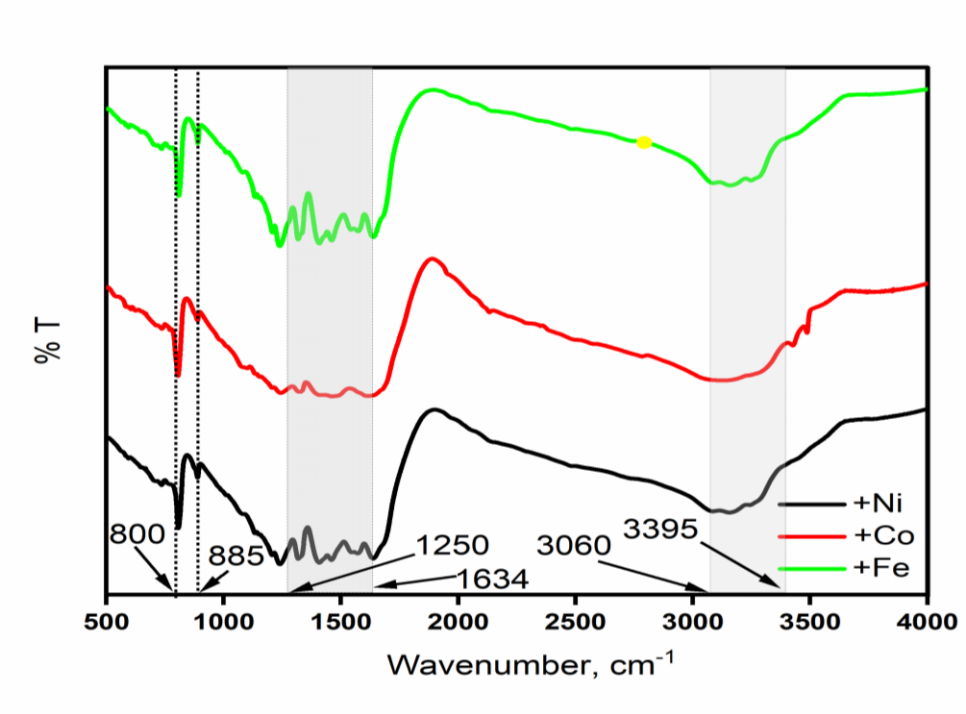

Figure 4.3 FTIR spectrum of g–C_3N_4/Fe, g–C_3N_4/Co and g–C_3N_4/Ni

Notably, the peak positions in the spectra of g–C_3N_4 doped with iron (g–C_3N_4/Fe) and cobalt (g–C_3N_4/Co) are identical in terms of wavenumber. However, they demonstrate differing transmittance values. This indicates that the transmission characteristics of g–C_3N_4/Fe are superior, exhibiting higher transmittance and an enhanced capacity for light absorption compared to g–C_3N_4/Co (Vandna et. al., 2024).

3.3 EDX

The EDX analysis depicted alterations in the elemental composition of g–C_3N_4 resulting from metal doping. Specifically, the increase in weight percentage (% wt.) for

the different metals was as follows: 1.64% for Ni, 0.22% for Co, and a notably higher 10.1% for Fe. This substantial rise in % wt. for Fe indicates that, when using the same precursor amount, the replacement of nitrogen atoms with iron atoms is most efficient. This conclusion is drawn from the significantly greater change observed in the case of Fe compared to Ni and Co. This shows iron (Fe) is more suitable than nickel (Ni) for doping photocatalysts like carbon nitride because of its ability to form stronger bonds with the photocatalyst and its favorable redox properties (Naldoni et al, 2013).

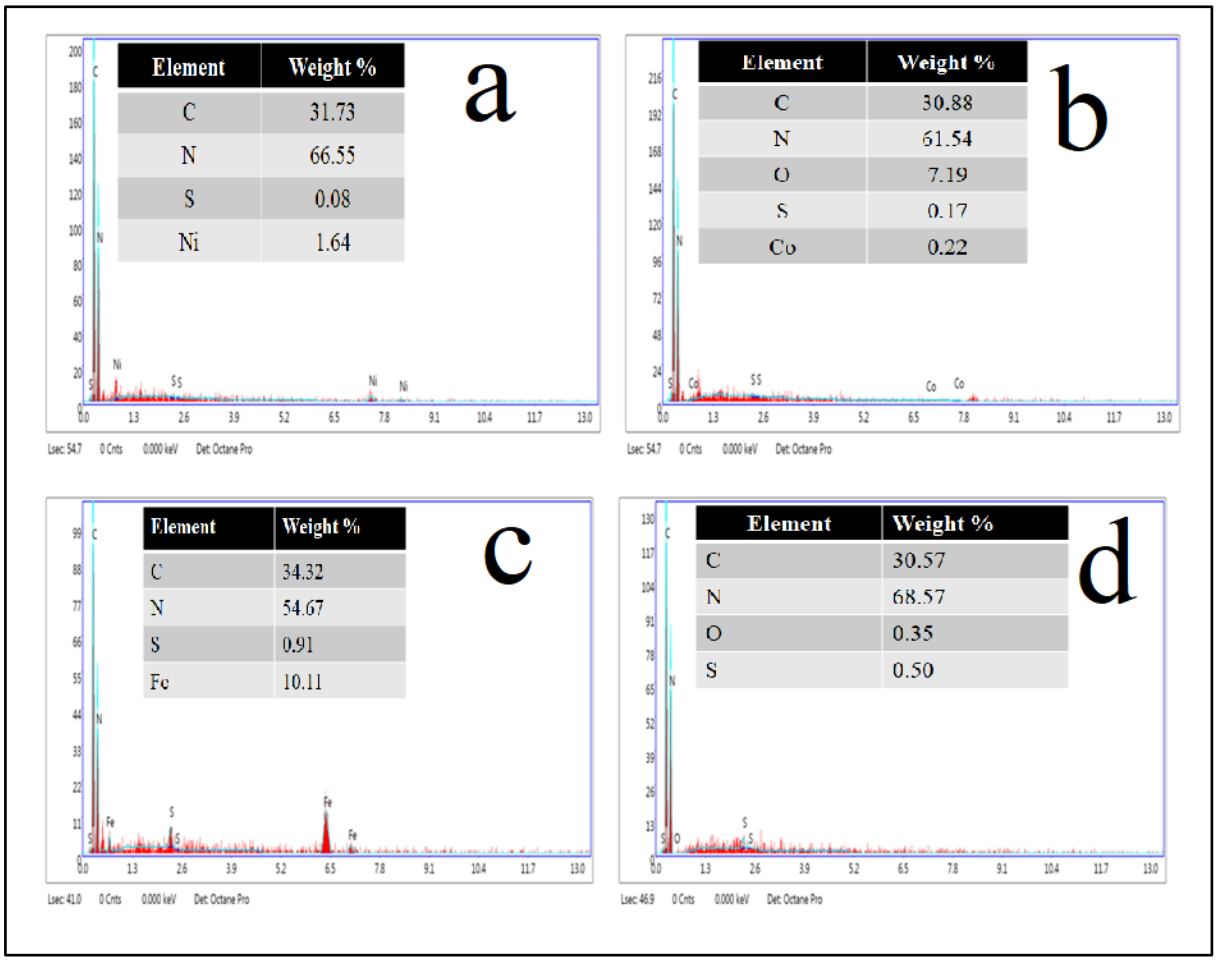

Figure 4.4 EDX spectrum of graphitic carbon nitride doped with (a) Ni (b) Co (c) Fe and (d) undoped

3.4 BET

Since g– C_3N_4 doped with iron showed best results in UV–Vis spectra among all three, further study is done with it like BET characterization, effect of three different parameters, catalyst dose, dye effects and light intensity. Both adsorption, as well as desorption are higher as compared to pure g–C_3N_4. Particle size and isotherm both revealed that photocatalyst form is mesoporous with an average diameter of ~35nm and formation of a monolayer on the surface of photocatalyst at p/p_0 = 0.2 to 0.8. Adsorption–desorption studies revealed that pore diameter is reduced from 33.9 nm to 31.612 nm, pore volume enhanced significantly from 0.157 to 0.287 cm^3/g and surface area ramped

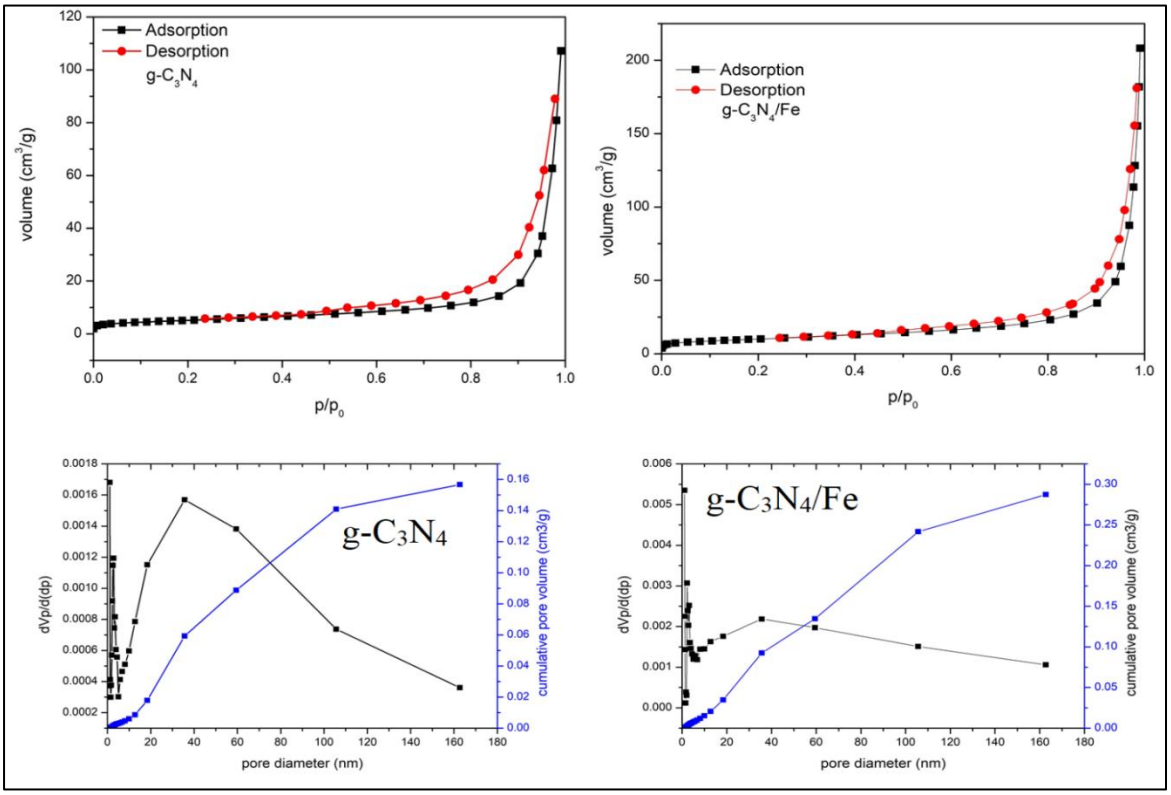

Figure 4.5 BET results: Adsorption–desorption isotherm at 77.36 K of (a) g–C_3N_4 and (b) g–C_3N_4/Fe; pore surface area of (c) g–C_3N_4 and (d) g–C_3N_4/Fe

to 36.372 m^2/g from 18.467 m^2/g. The effect of the hike in the surface area is reflected in gas adsorption (A. M. Devi et. al., 2022).

Increased pore volume will result in providing a better number of sites to undergo photocatalytic reaction and desorption isotherm depicts the availability of the site for photocatalytic reaction since almost all adsorbed molecules desorbed. Large number of particles in pore size distribution curve shows large number of particles is having small pore diameter in (c) and (d). However, gas adsorption is getting increased in case of g–C_3N_4/Fe from 100 cm^3/g to 200 cm^3/g as compared to pure g–C_3N_4 and cumulative pore volume is also doubled from 0.16 cm^3/g to 0.30 cm^3/g (J. Yu et. al., 2022).

Graphitic carbon nitride shows higher activity in UV and comparatively low in VL region although its activity was increased with the introduction of metal. Among the three metals, Fe showed higher activity under VL

Table 4.1 Percent removal for different catalyst

Catalyst	Removal by adsorption	Removal by photocatalysis
g–C_3N_4	0.20	0.21
g–C_3N_4/Ni	0.51	0.24
g–C_3N_4/Fe	0.15	0.60
g–C_3N_4/Co	0.25	0.35

Change in concentration of congo red dye solution (20 ppm) with time is depicted here corresponding to different metals doped in g–C_3N_4 and compared with pure g–C_3N_4. After the introduction of the catalyst, after 30 min light is turned on for the photocatalysis process. Before turning on the light adsorption on the surface of photocatalysts caused a dip in concentration due to the adsorption. After turning on the light, a photocatalysis

reaction started to occur. Findings showed that change due to adsorption is most in the case of Ni while photocatalysis caused further change in concentration and was maximum for g–C_3N_4 impregnated with Fe. Ni doped g-C_3N_4 showed removal in dark while in case of Fe doped, photocatalysis took place. This is probably due to: When nickel (Ni) is doped into photocatalysts, it enhances adsorption due to its ability to create new active sites on the surface. Additionally, ability of iron to exist in two major oxidation states (Fe^{2+} and Fe^{3+}) allows it to participate more efficiently in electron transfer processes, making it particularly suitable for photocatalysis and catalysis. The transition between these oxidation states is more easily facilitated in many systems, leading to better charge separation and enhanced catalytic activity . The intensity of light during the whole process is kept the same and the catalyst dose in the dye solution is also the same (Zheng et al, 2022).

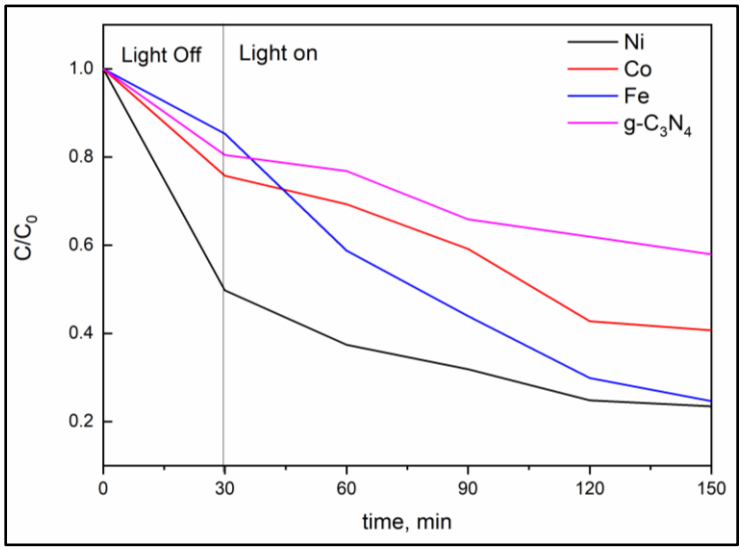

Figure 4.6 Dye degradation with time

4. Effect of some operating parameters

Here effect of light intensity, the dose of catalyst and dye concentration is varied & corresponding degradation is measured with iron doped catalyst

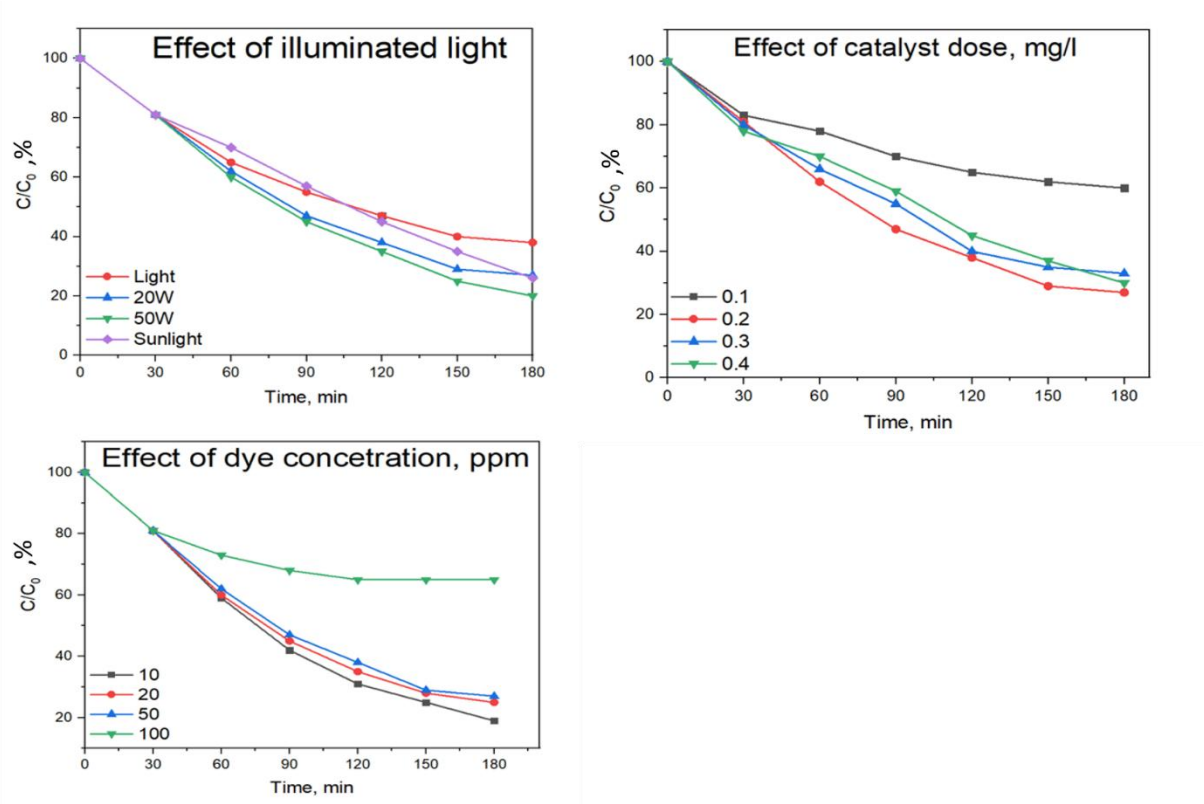

Figure 4.7 Effect of different parameters on g–C_3N_4/Fe

5. Degradation kinetics

In both the cases undoped and doped with iron, graphitic carbon nitride followed first-order kinetics. Just rate constant is slightly increased from 0.0055min^{-1} to 0.0077 min^{-1} with undoped and doped catalysts respectively.

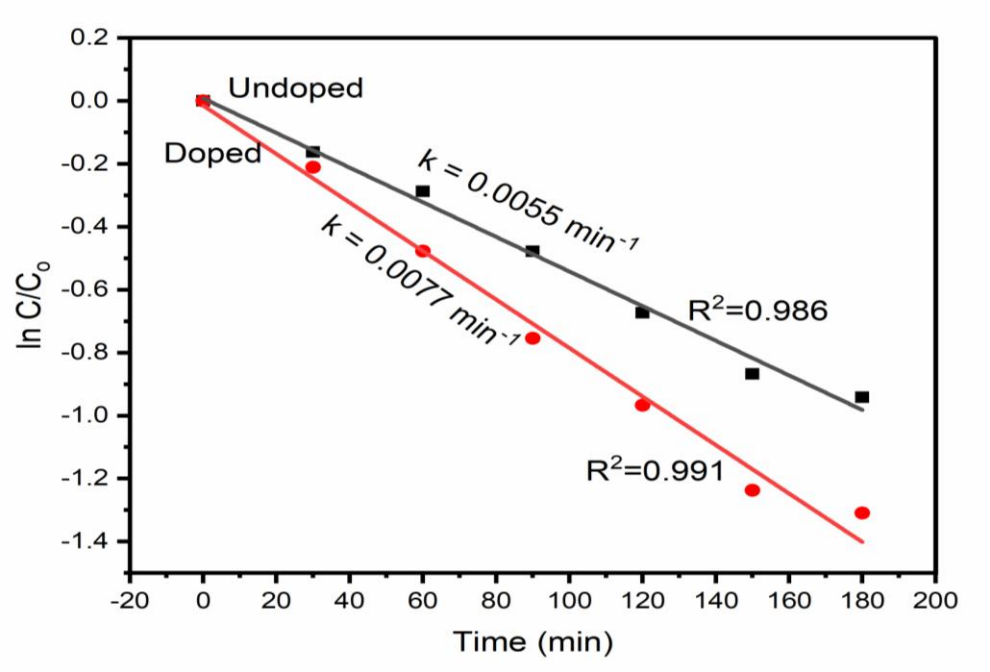

Figure 4.8 Rate order of iron doped g–C_3N_4 and undoped g–C_3N_4